

The Growth of Central and Satellite Galaxies in Cosmological Smoothed Particle Hydrodynamics Simulations

Vimal Simha¹, David H. Weinberg¹, Romeel Davé²,
Oleg Y. Gnedin³, Neal Katz⁴, Dušan Kereš⁵

¹ *Astronomy Department and Center for Cosmology and AstroParticle Physics, Ohio State University, Columbus, OH 43210, vsimha,dhw@astronomy.ohio-state.edu*

² *University of Arizona, Steward Observatory, Tucson, AZ 85721, rad@as.arizona.edu*

³ *Department of Astronomy, University of Michigan, MI 48109, ognedin@umich.edu*

⁴ *Astronomy Department, University of Massachusetts at Amherst, MA 01003, nsk@kaka.phast.umass.edu*

⁵ *Institute for Theory and Computation, Harvard-Smithsonian Center for Astrophysics, Cambridge, MA 02138, dkeres@cfa.harvard.edu*

23 October 2018

ABSTRACT

We examine the accretion and merger histories of central and satellite galaxies in a smoothed particle hydrodynamics (SPH) cosmological simulation that resolves galaxies down to $7 \times 10^9 M_\odot$. Most friends-of-friends haloes in the simulation have a distinct central galaxy, typically two to five times more massive than the most massive satellite. As expected, satellites have systematically higher assembly redshifts than central galaxies of the same baryonic mass, and satellites in more massive haloes form earlier. However, contrary to the simplest expectations, satellite galaxies continue to accrete gas and convert it to stars; the gas accretion declines steadily over a period of $0.5 - 1$ Gyr after the satellite halo merges with a larger parent halo. Satellites in a cluster mass halo eventually begin to lose baryonic mass. Since $z = 1$, 27% of central galaxies (above $3 \times 10^{10} M_\odot$) and 22% of present-day satellite galaxies have merged with a smaller system above a 1:4 mass ratio; about half of the satellite mergers occurred after the galaxy became a satellite and half before. In effect, satellite galaxies can remain “central” objects of halo substructures, with continuing accretion and mergers, making the transition in assembly histories and physical properties a gradual one. Implementing such a gradual transformation in semi-analytic models would improve their agreement with observed colour distributions of satellite galaxies in groups and with the observed colour dependence of galaxy clustering.

Key words: galaxies: evolution — galaxies: formation — models: semi-analytic — models: numerical

1 INTRODUCTION

In the standard theoretical description of galaxy formation, galaxies grow initially by the condensation of gas at the centres of dark matter potential wells (e.g. White & Rees 1978; Fall & Efstathiou 1980). When a large dark matter halo accretes a smaller halo, the galaxy hosted by the smaller halo becomes a satellite system, which may eventually merge with the central object after sinking by dynamical friction. Even if the satellite retains some of its original dark matter, it is likely to move through the large parent halo with a random velocity that exceeds its own escape speed, making it difficult for the satellite to ac-

crete gas from the halo or to merge with other satellites. In semi-analytic models of galaxy formation (e.g. White & Frenk 1991; Kauffmann, White & Guideroni 1993; Cole et al. 1994; Primack et al. 1998; Croton et al. 2006; Bower et al. 2006), these expected differences between central and satellite galaxies are usually encoded by simple rules, with some variations from one model to another. When two haloes merge, the central galaxy of the more massive progenitor becomes the central galaxy of the new, larger halo. Cooling gas from the halo is assigned mostly or entirely to the central galaxy. Satellites accrete little or no fresh gas, and their pre-existing gas may be removed by ram pres-

sure stripping when they enter the larger halo. Most or all mergers are assumed to involve satellites joining the central galaxy rather than merging with each other.

In this paper, we examine the growth of central and satellite galaxies in smoothed particle hydrodynamics (SPH) cosmological simulations (Katz, Hernquist, & Weinberg 1992; Evrard et al. 1994; Katz, Weinberg & Hernquist 1996). In such simulations, differences between central and satellite galaxies are not imposed a priori, but central galaxies nevertheless emerge as a distinct class for the physical reasons discussed above. The galaxy closest to the halo centre of mass is usually older and more massive than satellites in the same halo (Berlind et al. 2003; Zheng et al. 2005). Here we investigate the assembly histories of present day centrals and satellites as a function of galaxy and halo mass, and we track the growth of galaxies to see the extent to which satellite systems experience continuing gas accretion or mergers with other satellites.

Our goals are to understand the physics of galaxy assembly in the simulation and to inform semi-analytic models of galaxy formation and other efforts to interpret observed galaxy clustering and the environmental dependence of galaxy properties. The central-satellite distinction is a key element in modeling the origin of bimodality in the galaxy population, in which galaxies with old stellar populations and little ongoing star formation form a distinct, passive, “red sequence” (Strateva et al. 2001; Blanton et al. 2001; Bell et al. 2003; Faber et al. 2007). Strangulation of gas supplies in satellites is the likely route by which many galaxies join the passive sequence, though additional mechanisms are required to explain the red colours and low star formation rates of the most massive galaxies (see e.g. Croton et al. 2006; Dekel & Birnboim 2006; Cattaneo et al. 2007). Central-satellite separation is also a key ingredient in “halo occupation distribution” (HOD) models of galaxy clustering (Kravtsov et al. 2004; Zheng et al. 2005) and in recent efforts to interpret properties of galaxy groups (e.g. Weinmann et al. 2006; Gilbank et al. 2008; Hansen et al. 2007; Li et al. 2007; Coil et al. 2008).

The simulation that we analyse here is also the main simulation analysed by Kereš et al. (2005) and Maller et al. (2006), who examine gas accretion and merger rates but do not distinguish between central and satellite galaxies. Kereš et al. (2005) emphasise the distinction between between “cold” and “hot” modes of gas accretion. In haloes of total mass $M \leq 3 \times 10^{11} M_{\odot}$, most gas that accretes onto galaxies does so without ever heating close to the halo virial temperature. In higher mass haloes, most gas heats to the virial temperature before settling into galaxies. Overall, about half of the baryonic mass in the simulation’s $z = 0$ galaxy population was originally accreted in “cold mode” and half in “hot mode”, with the former dominating at high redshift and in low mass galaxies today. Here we will investigate both total and cold-only accretion rates of central and satellite systems. Further discussions of the cold/hot dichotomy appear in Binney (1977), Binney (2004), Katz (1992), Kay et al. (2000), Fardal et al. (2001), Katz et al. (2003), Birnboim & Dekel (2003), Croton et al. (2006), Dekel & Birnboim (2006) and Kereš et al. (2008).

We describe our simulation and methods for identifying haloes and galaxies in §2, before proceeding to our main results in §3. There we start with a qualitative overview of ac-

cretion and merger properties of central and satellite galaxies, then quantify their relative accretion rates and merger rates and their dependences on halo mass. In §4 we summarise our results and discuss their implications, with particular attention to recent studies of galaxy bimodality and the red population in groups.

2 SIMULATION AND NUMERICAL METHODS

2.1 Simulation

Our simulation is performed using a parallel implementation of TreeSPH (Davé et al. 1997; Hernquist & Katz 1989; Katz, Weinberg & Hernquist 1996), which combines a tree algorithm for gravitational calculations with smoothed particle hydrodynamics (SPH). There are three kinds of particles in our simulation: dark matter, stars and gas. The collisionless particles (dark matter and stars) are influenced only by gravity, whereas the gas particles are influenced by pressure gradients and shocks in addition to gravity. Gas particles experience adiabatic heating and cooling, shock heating, inverse Compton cooling off the CMB and radiative cooling via free-free emission, collisional ionisation and recombination and collisionally excited line cooling. Further details of the code can be found in Katz, Weinberg & Hernquist (1996).

We model a comoving $22.222h^{-1}$ Mpc periodic box with 128^3 gas particles and 128^3 dark matter particles. The dark matter particle mass is $7.9 \times 10^8 M_{\odot}$, and the SPH particle mass is $1.05 \times 10^8 M_{\odot}$. The gravitational force softening is a comoving $5h^{-1}$ kpc cubic spline, which is roughly equivalent to a Plummer force softening of $3.5h^{-1}$ kpc.

We include star formation as described by Katz, Weinberg & Hernquist (1996). Overdense, Jeans unstable gas that is part of a converging flow with density $\rho_{\text{gas}} > 0.1m_{\text{Hcm}}^{-3}$ and temperature $T \leq 30,000\text{K}$ is converted to stars on a timescale set by the dynamical timescale or the cooling time, whichever is longer. Our prescription for star formation leads to a relation with gas surface density similar to a Schmidt law. We adopt a Miller & Scalo (1979) initial mass function. We include supernova feedback with 7.35×10^{-3} supernovae per solar mass, and each supernova deposits 10^{51} ergs of energy into the surrounding medium. Since the surrounding gas is dense, this energy is usually radiated away before it can drive outflows or suppress subsequent star formation.

We adopt a Λ CDM cosmology (inflationary cold dark matter with a cosmological constant) with $\Omega_m=0.4$, $\Omega_{\Lambda}=0.6$, $h=0.65$, $\Omega_b = 0.02h^{-2}$, spectral index $n=0.93$, and $\sigma_8=0.8$. These values are reasonably close to the estimates from the cosmic microwave background (Dunkley et al. 2008) and large scale structure (Tegmark et al. 2006), though these favour somewhat lower Ω_m (≈ 0.25) and higher h (≈ 0.7). We do not expect modest differences in cosmological parameters to influence our conclusions.

Hydrodynamic cosmological simulations produce dense groups of baryons with sizes and masses comparable to the luminous regions of observed galaxies (Katz 1992). We identify galaxies using the Spline Kernel Interpolative DENMAX (SKID) algorithm (Gelb & Bertschinger 1994;

Katz, Weinberg & Hernquist 1996), which identifies gravitationally bound particles associated with a common density maximum. We apply this algorithm to all baryonic particles with $T < 3 \times 10^4 K$ and $\rho_{\text{gas}}/\bar{\rho}_{\text{gas}} > 10^3$, and we refer to the groups of stars and cold gas thus identified as galaxies. The simulated galaxy population becomes substantially incomplete below our resolution threshold of 64 SPH particles (Murali et al. 2002), which corresponds to a baryonic mass of $6.8 \times 10^9 M_{\odot}$. We ignore lower mass galaxies in our analysis. There are 1120 galaxies above the resolution threshold in our simulation.

We identify dark matter haloes using a FOF (friends-of-friends) algorithm (Davis et al. 1985). The algorithm selects groups of particles in which each particle has at least one neighbour within a linking length. We adopt a linking length $l = 0.2\bar{n}^{-1/3}$, where \bar{n} is the mean dark matter particle density, which leads to haloes with typical mean overdensity $\rho/\bar{\rho} \approx 200$. By chance, the simulation contains one halo that is anomalously massive ($M_h = 3.4 \times 10^{14} M_{\odot}$) for the simulation volume, which has some impact on our statistics for satellite galaxies when these are not broken down into halo mass bins.

We use 227 output epochs between $z = 9$ and $z = 0$, with a typical spacing between output epochs of less than 150 Myr. At each epoch, we identify haloes and galaxies above the resolution threshold.

2.2 Central and satellite galaxies

Figure 1 shows a selection of six FOF haloes and their galaxy populations at $z = 0$. Each panel is centred on the most bound dark matter particle in the halo. The centre of mass is shown as a red filled circle in the figure. The galaxies are shown as open circles with areas proportional to their (baryonic) mass. A large majority of haloes have a clear central galaxy that is more massive than other galaxies in the halo and located at the bottom of the dark matter potential well. However, in a small number of haloes there are two galaxies of comparable mass, each with its own satellites. Some of the systems without a clear central galaxy consist of distinct sub-groups that are in the process of undergoing a merger, as in the lower left panel of Figure 1.

We hereafter define the central galaxy of each halo to be the galaxy with the largest baryonic mass. Inspection of many haloes shows that this identification is always reasonable when the halo is regular, and as reasonable as any other choice for the small fraction of irregular haloes.

Figure 2 shows the masses of galaxies and haloes in the simulation. The left hand panel plots galaxy mass versus halo mass, with central galaxies shown as filled squares and satellite galaxies shown as open circles. The right hand panel plots the distribution of M_1/M_0 , where M_0 is the mass of the central galaxy and M_1 is the mass of the most massive satellite. We omit haloes that have no satellites above the resolution threshold. The distribution of satellite mass ratios is broad, and more than two-thirds of haloes have $0.2 \leq M_1/M_0 \leq 0.5$. Only a small fraction of haloes have two galaxies of comparable mass ($M_1/M_0 \geq 0.8$).

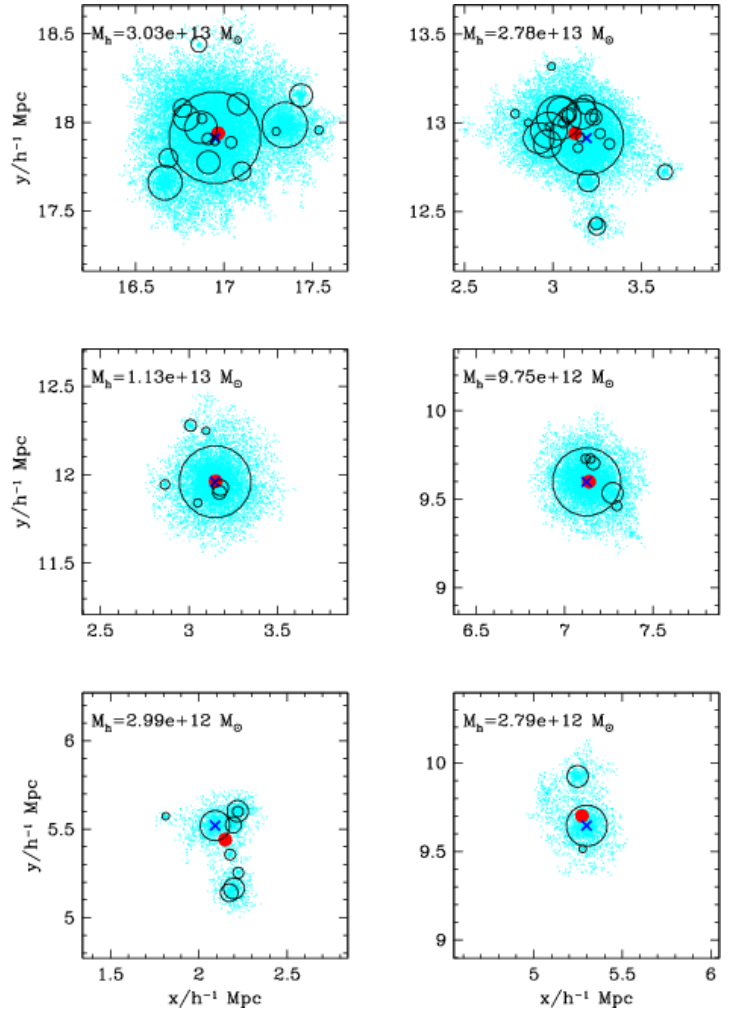


Figure 1. A selection of friends-of-friends haloes and their galaxy populations. The small blue dots are dark matter particles, the galaxies are shown as open black circles with their areas proportional to their masses. Each panel is centred on the most bound dark matter particle shown as a blue cross, and the centre of mass of the dark matter particles is shown as a red filled circle.

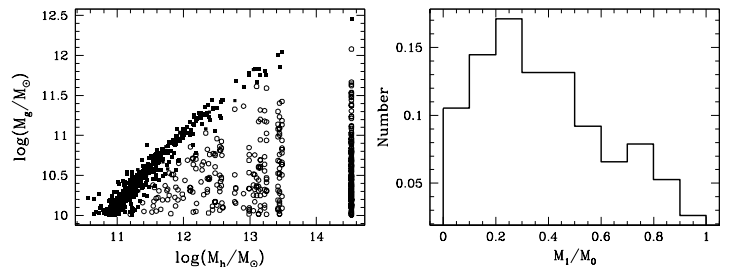


Figure 2.

(Left) Masses of central galaxies (squares) and satellite galaxies (circles) plotted against halo mass. (Right) A histogram of the ratio of the mass M_1 of the most massive satellite galaxy to the mass M_0 of the central galaxy.

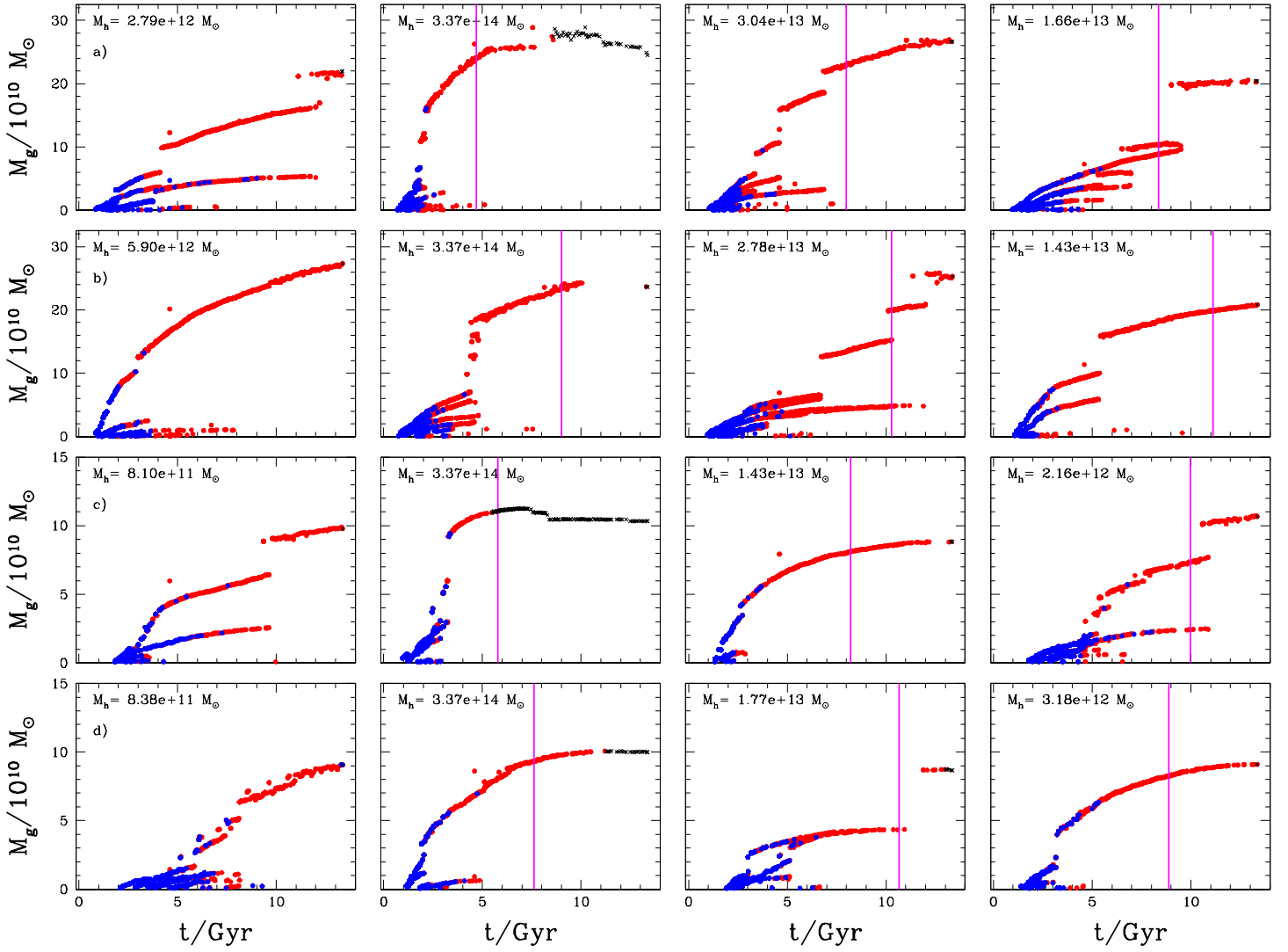


Figure 3. Evolution of galaxies with time. Cold accretion is shown in blue and hot accretion in red. M_h (top left corner) is the halo mass. The black crosses show the subsequent evolution of the mass of the galaxy after its last accretion event. For the satellite galaxies, the magenta coloured vertical line marks the epoch at which it became a satellite. The first column shows central galaxies, while columns 2, 3 and 4 show satellite galaxies in decreasing order of halo mass. Panels (a) and (b) show galaxies with masses of $\sim 3 \times 10^{11} M_\odot$ while panels (c) and (d) show galaxies with masses of $\sim 10^{11} M_\odot$.

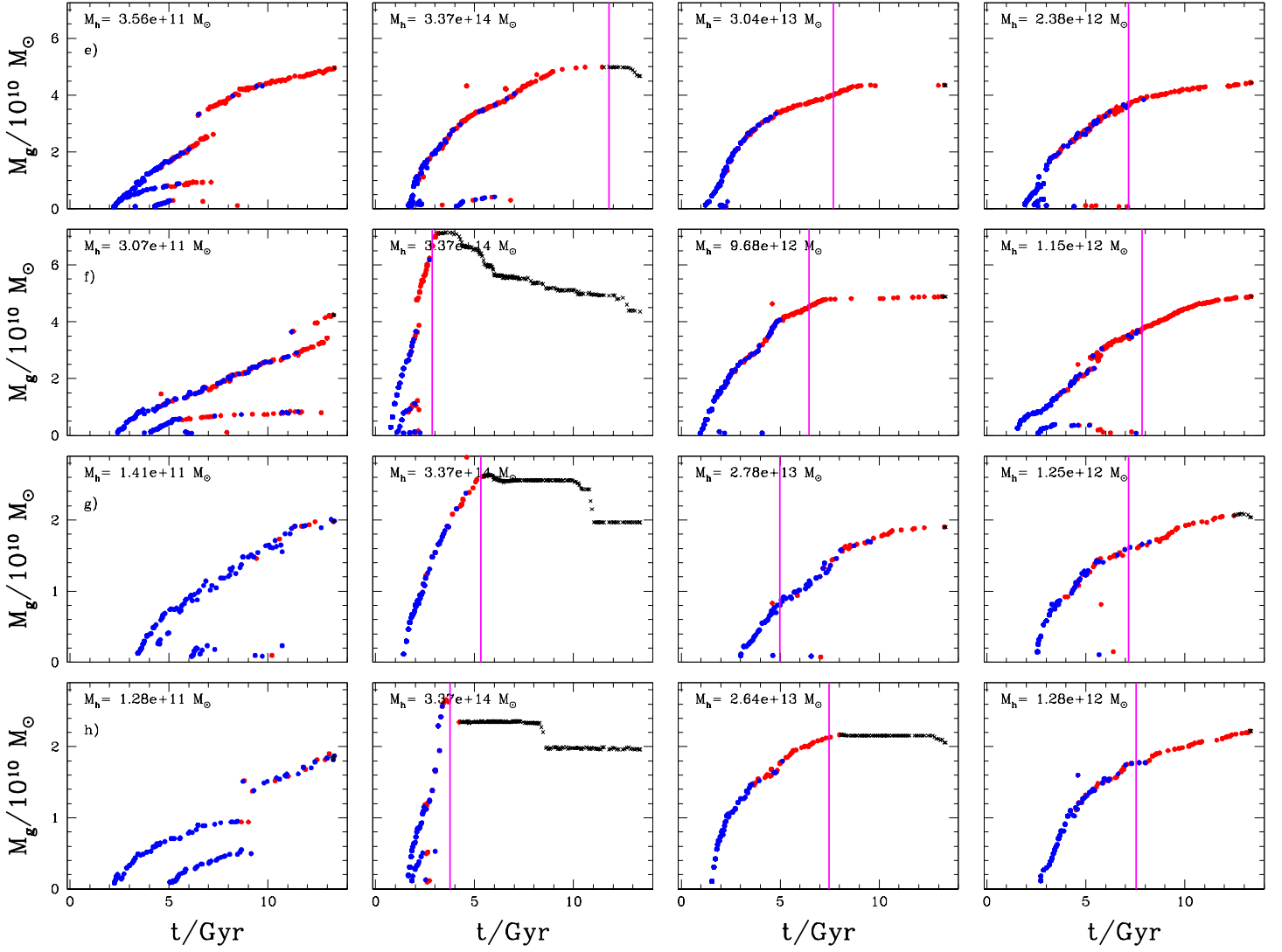


Figure 3(continued) Panels (e) and (f) show galaxies with masses of $\sim 5 \times 10^{10} M_\odot$ while panels (g) and (h) show galaxies with masses of $\sim 2 \times 10^{10} M_\odot$.

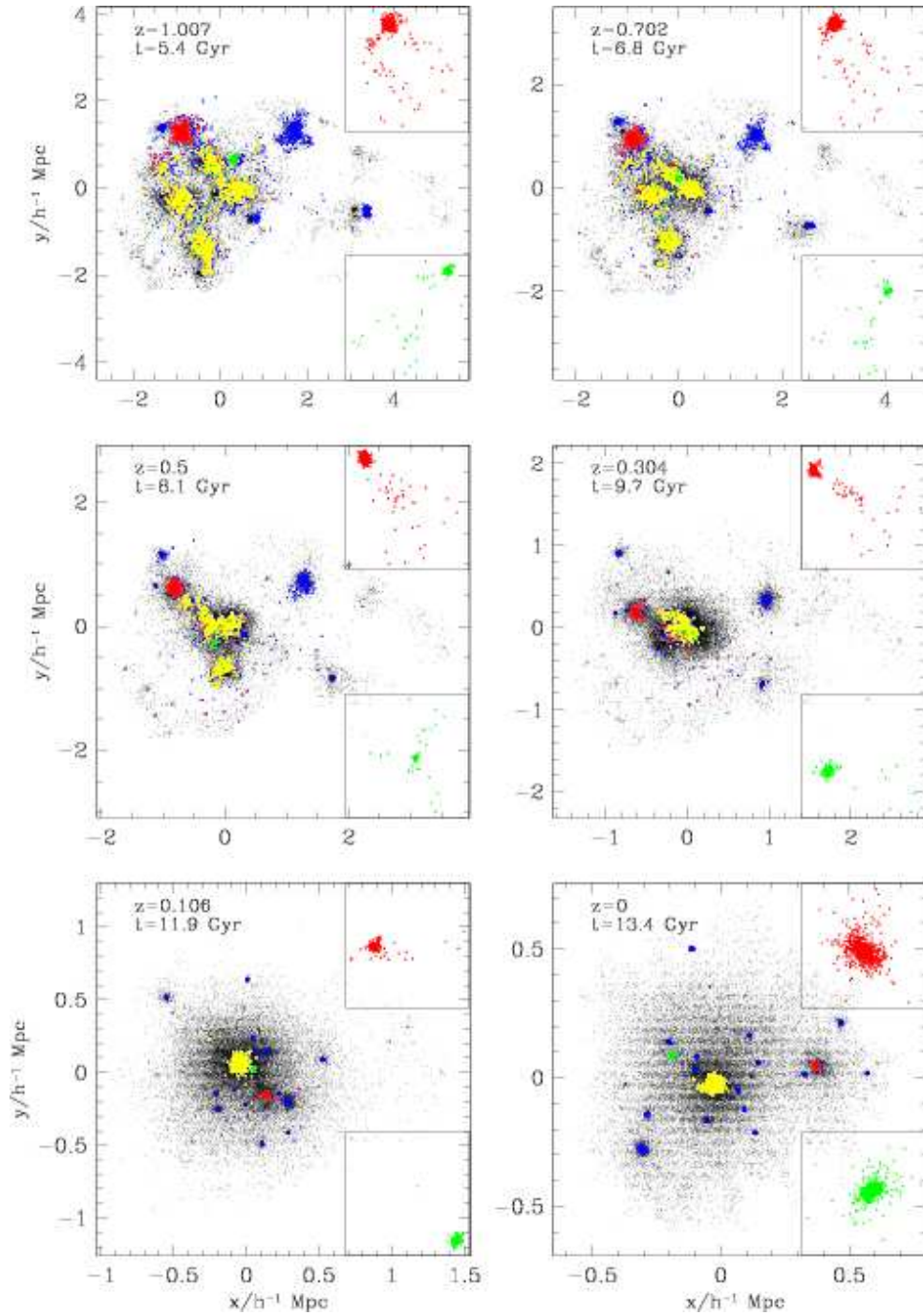


Figure 4. The evolution of a $3 \times 10^{13} M_{\odot}$ halo with redshift, with positions marked in comoving h^{-1} Mpc. Dark matter particles are shown as black dots. The particles in the central galaxy at $z = 0$ are shown in yellow. The red galaxy is the most massive satellite galaxy, which becomes a satellite at $z = 0.514$, while the green galaxy becomes a satellite at $z = 0.736$. The baryonic particles of other $z = 0$ satellites are shown in blue. The inset panels in the right hand corners show a magnification of the red and green satellites, large enough to encompass all of their member particles. While the central galaxy has a large total extent at $z = 0$, its stellar half-mass radius is only $3.9 h^{-1}$ kpc.

3 ACCRETION AND MERGER PROPERTIES: CENTRAL AND SATELLITE GALAXIES

Figure 3 shows the assembly history of a representative sample of central and satellite galaxies. At each of our 227 output epochs from the simulation, we use SKID to identify galaxies with at least 8 SPH particles. For galaxies resolved in two consecutive output epochs, we identify gas particles that are in the galaxy at the later epoch but are not in any resolved galaxy at the earlier epoch as smoothly accreted gas. In Figure 3, galaxy mass is shown on the vertical axis, and time is shown on the horizontal axis. Each point represents an accretion event, showing the baryonic mass of the SKID identified galaxy when the particle was accreted onto it. Every particle that is in the $z = 0$ group is shown. The locus traced by the topmost points shows the growth of the most massive progenitor of the $z = 0$ galaxy, while lower ridges trace the growth of secondary progenitors which merge onto the main progenitor (or with each other) producing jumps in the mass track. There are occasional outlier points, cases in which an accreting particle is incorrectly assigned to a more massive neighboring system instead of the galaxy in which it is actually located.

Following Kereš et al. (2005), we distinguish between cold and hot accretion. We trace the temperature history of each particle and identify the maximum temperature T_{\max} that the particle had prior to accreting onto a galaxy since the beginning of the simulation. Particles with $T_{\max} \leq 2.5 \times 10^5 \text{K}$ are classified as cold and shown in blue colour, and particles with $T_{\max} \geq 2.5 \times 10^5 \text{K}$ are classified as hot and shown in red. Since each point corresponds to accretion of one particle, intermediate mass galaxies sometimes show interleaved hot and cold accretion events.

For satellite galaxies, we trace the history of its most massive progenitor galaxy and identify the epoch when it became a satellite, which we define as the epoch when the parent halo of the satellite merges with the parent halo of a more massive galaxy. In Figure 3, the magenta coloured vertical line marks the epoch when the galaxy became a satellite.

Rows (a) and (b) of Figure 3 show high mass galaxies with final baryonic masses (consisting of stars and cold, dense gas) of $M_g \sim 2 - 3 \times 10^{11} M_\odot$. Subsequent rows show galaxies with final baryonic masses $M_g \sim 10^{11} M_\odot$ (c and d), $M_g \sim 4 - 5 \times 10^{10} M_\odot$ (e and f) and $M_g \sim 1 - 2 \times 10^{10} M_\odot$ (g and h). In each row, the first column shows a central galaxy in a halo of mass $M_h \sim 5 - 10 M_g$. Subsequent columns show satellite galaxies in decreasing order of halo mass. The second column shows satellite galaxies selected from the most massive halo in the simulation ($M_h = 3.4 \times 10^{14} M_\odot$). The third and fourth columns show satellite galaxies from intermediate mass haloes and low mass haloes respectively. While these thirty-two examples cannot capture the full range of assembly histories that we see in the simulation, they suffice to illustrate the main qualitative trends.

An examination of Figure 3 reveals a number of interesting trends. The assembly of high mass galaxies is complex, with active merger histories and continuing accretion at late times. Among high mass galaxies, there is not much difference between the assembly histories of central galaxies and satellite galaxies, except for the satellites in the most massive halo. Satellites in intermediate mass haloes, as shown in

columns 3 and 4, continue to accrete gas and form stars after z_{sat} , the epoch when they become satellites. Some systems, such as the galaxy in the third column of row (b) and the fourth column of rows (a) and (c), “receive” mergers after becoming satellites. However, satellites in the highest mass halo are an exception. For these, assembly occurs early and there is little accretion after z_{sat} , and there is mass loss in some cases such as row (c) column 2.

The assembly of lower mass galaxies appears to be smoother with fewer merger events. However, because our galaxy population is incomplete below our resolution threshold of $6.8 \times 10^9 M_\odot$, it is likely that we miss many lower mass merger events. Lower mass galaxies in low and intermediate mass haloes often have continuing accretion and star formation after becoming a satellite, with row (g), column 3 being a striking example. Some lower mass galaxies in intermediate mass haloes, such as column 3 of rows (e) and (f), have low but non-zero accretion rates at late times. The assembly histories of low mass galaxies in the most massive halo are systematically different from their central counterparts. They experience very little accretion after becoming satellites, and in many cases they experience significant mass loss (column 2 of rows f-h).

Overall, Figure 3 shows surprisingly little distinction between central and satellite galaxies. Galaxy mass is generally a stronger predictor of growth history than central/satellite status. We do see some trends of the expected sign, but z_{sat} , when the galaxy becomes a satellite, is not a sharp boundary in the accretion or merger history. Satellites in the most massive halo are an exception, in that accretion is slowed or shut-off at z_{sat} , and some satellites experience mass loss. We have examined assembly histories of many more systems in addition to the 32 shown in Figure 3, and they confirm the qualitative points made here.

It is remarkable that satellites in low and intermediate mass haloes, which are moving at high velocities in the potential of the halo, continue to accrete gas and form stars. Our conjecture is that continuing accretion by satellites owes to substructure in the haloes. In effect, a satellite galaxy in a large halo may still be the central galaxy of its own coherent sub-group. Figure 4 investigates one such system, a $3 \times 10^{13} M_\odot$ halo as it evolves from $z = 1.07$ to $z = 0$. We plot the dark matter particles in black and the baryonic particles in different colours, which depend on their galaxy membership at $z = 0$. Figure 5 shows the corresponding assembly histories of the eight most massive galaxies in this halo. Consider the most massive satellite galaxy, shown in red in Figure 4 (and in panel b of Figure 5). It starts off as a central galaxy in its own halo. Following the merger of its parent halo with the parent halo of the central galaxy at $z = 0.514$, it continues to accrete gas from the region around it and has other galaxies gravitationally bound to it, in effect its own satellites. Even at $z = 0$, it is the central object of a distinctly defined dark matter substructure. Hence, accretion is not shut off at z_{sat} , and there is no sharp transition in its behaviour at this redshift. Another satellite galaxy, shown in green in Figure 4, becomes a satellite at $z = 0.736$, but it receives a merger after that time.

We now turn to statistical measures to quantify the anecdotal results seen in Figures 3-5. Figure 6 compares the assembly histories of central and satellite galaxies as a function of galaxy mass and parent halo mass. For four galaxy

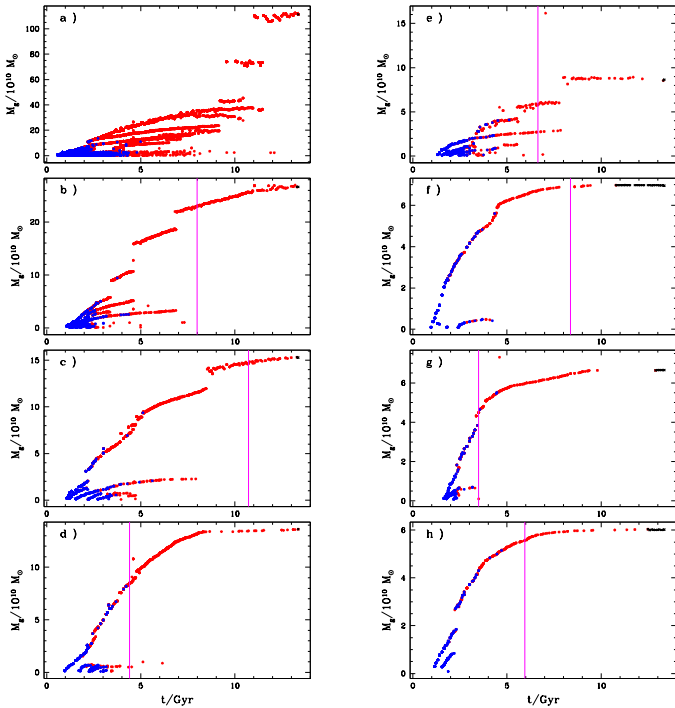


Figure 5. Galaxy mass vs time for galaxies in the halo of Figure 4. Panel (a) is the central galaxy, (b) is the most massive satellite, shown in red in Figure 4 and (e) is the satellite shown in green in Figure 4. The format is the same as figure 3

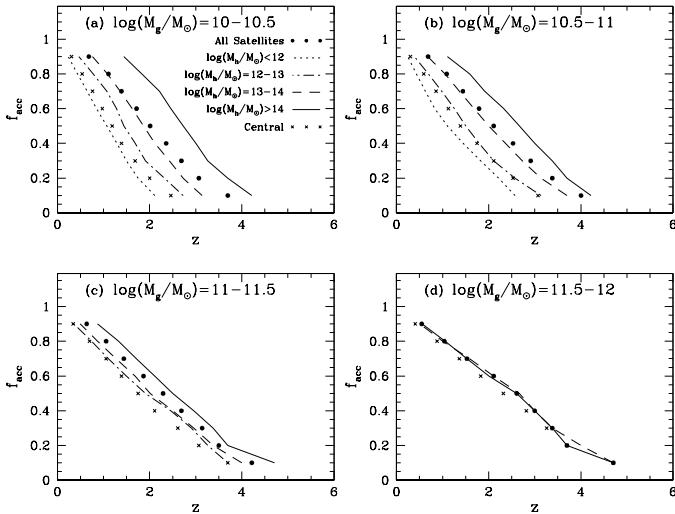


Figure 6. Fraction of final mass accreted by redshift z is plotted against redshift. We include mass in all progenitors of the $z = 0$ system. In each panel, crosses show accretion histories of central galaxies, circles show all satellites, and lines show satellites in bins of halo mass as indicated in the legend of panel (a).

mass bins, we plot the mass accreted by redshift z onto any of a galaxy’s SKID-identified progenitors divided by the total mass accreted up to $z = 0$. In each panel, the crosses show the results for all the central galaxies, the circles show all the satellite galaxies, and the lines show the satellites in different bins of halo mass.

Looking first at central galaxies, there is a clear trend

for higher mass galaxies to assemble at higher redshifts. For example, the redshift at which 50% of the final galaxy mass has been accreted by the central galaxy population ($f_{\text{acc}}=0.5$ in Figure 6) falls from $z = 2.2$ for $M_g = 10^{11.5}M_\odot$ - $10^{12}M_\odot$ to $z = 1.2$ for $M_g = 10^{10.5}M_\odot$ - $10^{11}M_\odot$, with a steady trend in between these masses. This downward shift of assembly redshifts is consistent with the well known “downsizing” trend of observed galaxy evolution. It arises naturally: massive galaxies reside in dense environments with accelerated early formation (Neistein et al. 2006). However, even the most massive galaxies have a significant fraction of mass accreted at low redshift, which is inconsistent with the observed red colours of the most massive galaxies.

Low mass satellite galaxies accrete most of their mass early on and experience little accretion at late times, with $f_{\text{acc}}=0.5$ at $z = 2$ compared to $z = 1.3$ for low mass centrals. There is a strong trend with halo mass: low mass satellites in the most massive halo assemble earlier and have accreted 90% of their final mass by $z = 1.5$, while the satellites in $M_h \leq 10^{12}M_\odot$ haloes have slightly lower assembly redshifts than comparable central galaxies. The same trends are seen for higher galaxy masses, but the differences between central and satellite galaxies are smaller. For high galaxy masses (panels c and d), there are no satellites in low mass haloes.

With our star formation prescription, which results in an increasing star formation rate with increasing gas density, star formation closely tracks the accretion of gas with a time lag (see Kereš et al. 2008). We find similar trends for star formation as we did for gas accretion: satellite galaxies typically form their stars earlier than central galaxies, but the difference is smaller at higher galaxy masses. Among satellites, those in high mass haloes typically form stars early on and have little star formation at late times, while satellites in low mass haloes continue to form stars at low redshifts.

To further investigate the physical processes involved in gas accretion by satellites, we differentiate between hot and cold accretion (Kereš et al. 2005). There are two reasons that it is interesting to isolate the contribution of cold accretion to galaxy growth. First, tests by Kereš (2007) and Kereš et al. (2008) show that the rate of hot gas accretion in hydrodynamic cosmological simulations is sensitive to differences among simulation codes but the cold accretion rates are robust. In particular, hot accretion rates are lower in simulations with GADGET (Springel et al. 2001) than in simulations with the PTreeSPH code used here, probably because the former employs an entropy conserving formulation of SPH. Second, AGN feedback, which is not incorporated in our simulation, could be more effective at suppressing hot accretion flows, since they have low-densities and are quasi-spherical compared to cold accretion flows, which channel dense gas along filaments (Kereš et al. 2005). Thus, for either numerical or physical reasons, the cold accretion rate in our simulation might be a better approximation to a galaxy’s true total accretion rate.

Figure 7 shows the fraction of $z = 0$ galaxy mass that was originally acquired (by the galaxy or its progenitors) via cold accretion. In agreement with Kereš et al. (2005), we find that low mass galaxies gain their mass almost entirely from cold accretion, while the highest mass galaxies gain up to 2/3 of their final mass by hot accretion. (This latter behaviour is different in the Gadget-2 simulations of Kereš et al.[2008], but the former remains true; see their Fig-

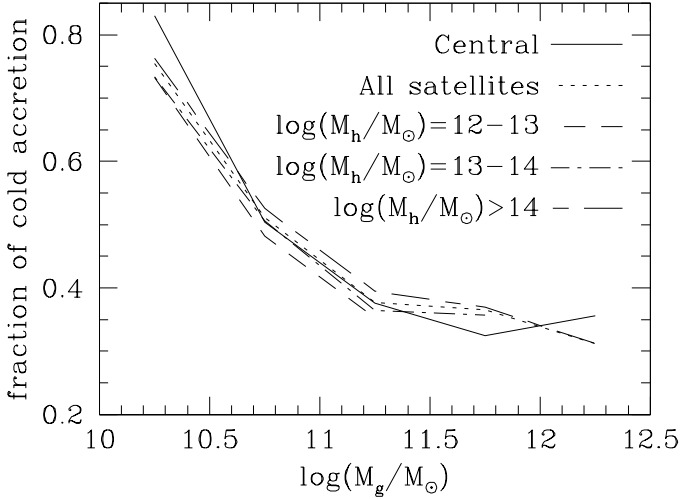


Figure 7. The fraction of $z = 0$ galaxy mass that was gained through cold accretion, as a function of galaxy mass. The solid line shows central galaxies, the dotted line shows all satellite galaxies and other lines show satellite galaxies in bins of halo mass as indicated in the legend.

ure 10.) Figure 7 shows that the trend with galaxy mass is nearly identical for central and satellite galaxies, and that among satellite galaxies there is no dependence of the cold accretion fraction on halo mass. If hot accretion were completely suppressed in the real universe (or in numerical simulations with a different treatment of gas physics or feedback), then to a first approximation the $z = 0$ galaxy masses would be reduced, on average, by the factor shown in Figure 7.

Figure 8 repeats the assembly history analysis of Figure 6, but we now eliminate all material gained originally through hot accretion (onto the galaxy or any of its progenitors) before computing galaxy masses at any redshift. All of the trends seen in Figure 6 are still apparent: assembly shifts towards higher redshifts for higher galaxy masses, satellite galaxies assemble earlier than central galaxies of the same mass, and satellites in massive haloes assemble earlier than satellites in low mass haloes. However, the trend of assembly history with galaxy mass is much stronger (for centrals and satellites) because galaxies experience little cold accretion once their mass exceeds $M_g \sim 3 \times 10^{10} M_\odot$ (Kereš et al. 2005). Galaxies above $M_g = 10^{11} M_\odot$ have typically accreted 90% of their final mass by $z = 2$. Suppressing hot accretion is thus a way of turning the most massive galaxies “red and dead” (Binney 2004; Croton et al. 2005; Kereš et al. 2005; Dekel & Birnboim 2006; Cattaneo et al. 2007).

So far, we have compared the properties of central galaxies to the properties of satellite galaxies over the course of their lifetime, from the time of their formation until $z = 0$. However, these satellites were once central galaxies, and they only become satellites at the redshift z_{sat} , when their parent halo merged with the parent halo of a more massive galaxy. To fairly compare the post- z_{sat} growth of satellites to central galaxies, we create a “control” sample. We associate each satellite galaxy above the resolution threshold with a randomly chosen central galaxy of similar baryonic mass. We follow the evolution of this matched central galaxy from z_{sat} of the corresponding satellite galaxy to $z = 0$. Thus,

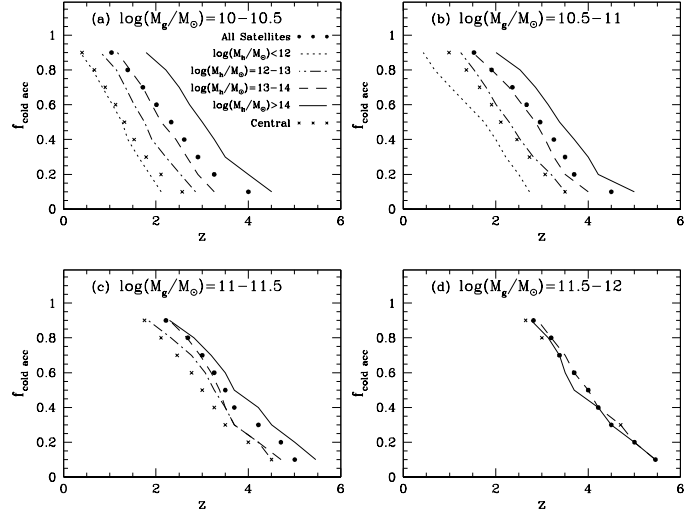


Figure 8. Fraction of mass accreted in the cold mode vs redshift. This figure is analogous to Figure 6, but we eliminate all material accumulated through hot accretion.

the control sample has the same mass distribution as the satellites and is traced over the same range of redshifts.

Figure 9 compares the mass accreted by satellite galaxies after they become satellites to the mass accreted by the control sample of central galaxies over the same time period. Panel (a) shows the mass accreted by each satellite galaxy from z_{sat} to $z = 0$ as a fraction of its mass at z_{sat} . Satellite galaxies in four halo mass bins are represented by different colours and point shapes. For comparison, we show the mass accreted by our control sample of central galaxies over the same time interval. Central galaxies tend to gain mass after z_{sat} of their matched satellites, with some even tripling their mass between z_{sat} and $z = 0$. For satellites, there is a trend with halo mass. Satellites in low mass haloes ($M_h \leq 10^{12} M_\odot$) gain a small fraction of their mass after z_{sat} . Satellites in intermediate mass haloes ($M_h = 10^{12} - 10^{14} M_\odot$) tend neither to lose nor gain much mass; their mass at $z = 0$ is similar to their mass at z_{sat} . Satellites in the high mass, $M_h = 4 \times 10^{14} M_\odot$ halo typically lose mass, in some cases up to half the mass they had at z_{sat} . The continuous nature of the trend with halo mass is more evident in panel (b), which presents histograms of the accreted mass fractions summed over all galaxy mass bins.

Panel (c) shows the mass accreted by galaxies in the cold mode from z_{sat} to $z = 0$, again scaled to the mass at z_{sat} (which still includes hot mode accretion up to that epoch). As in panel (a), we show satellite galaxies differentiated by halo mass, and we use the same control sample of central galaxies. For low mass galaxies, most of the accretion takes place in the cold mode. Hence, for low mass galaxies, panel (c) is identical to panel (a). However, for higher mass galaxies most of the accretion takes place through the hot mode, so above $M_g \sim 10^{10.5} M_\odot$ the accretion rates are lower for both central and satellite galaxies. As before, panel (d) presents histograms summed over bins of galaxy mass. It is again clear that central galaxies tend to gain mass after the matched z_{sat} and that satellites in the most massive halo tend to lose mass. However, with the lowered satellite accretion rates, the continuous trend in intermediate mass haloes

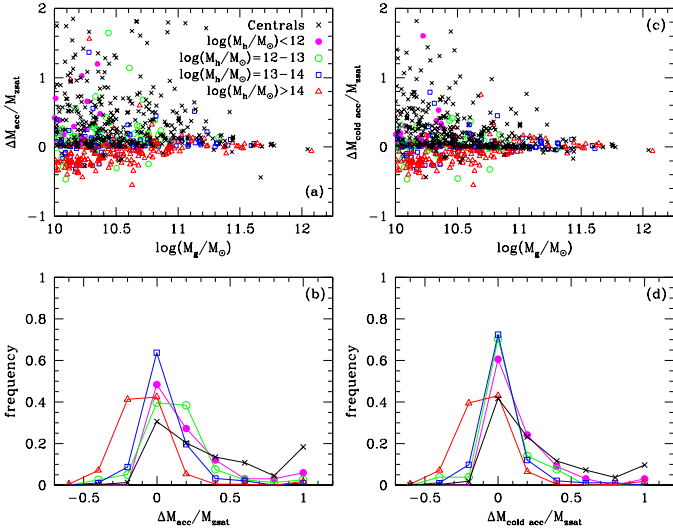


Figure 9. (Left) Mass change from accretion after becoming a satellite as a function of galaxy mass. Each point represents a galaxy. The red triangles, blue squares, green open circles and magenta filled circles show satellites in haloes of different masses. Each satellite galaxy is paired with a central galaxy of similar mass which is shown as a cross. M_g is the mass of the galaxy at $z = 0$. $M_{z_{\text{sat}}}$ is the mass of all the progenitors of the galaxy at the epoch when the most massive progenitor became a satellite. Panel (b) shows a histogram of the fractional mass change from accretion for satellites in different halo mass bins as well as central galaxies. (To preserve visual clarity, we plot this histogram as connected points.) (Right) Mass change from cold accretion after becoming a satellite. Panel (d) shows a histogram of the fractional mass change from cold accretion for satellites in different halo mass bins as well as central galaxies.

is no longer so clear - there is only a small amount of satellite accretion in the cold mode, even in relatively low mass haloes.

In our preceding analysis, we examined the mass accreted from z_{sat} to the present time and found differences in the total amount of accretion between central and satellite galaxies. To examine the timescale over which these differences develop, we define a dimensionless accretion rate as follows:

$$\eta = \frac{\Delta M_{\text{acc}}}{M_g} \frac{H^{-1}}{\Delta t}, \quad (1)$$

where ΔM_{acc} is the mass accreted in time interval Δt , H is the Hubble parameter evaluated at the centre of the time interval, and M_g is the mass of the galaxy at $z = 0$. For each epoch, we take a small time interval around the central epoch and calculate the accretion rate using the mass accreted, ΔM_{acc} and the time interval Δt between those epochs. The precise interval Δt depends on the simulation outputs available near z_{sat} , but typically $\Delta t \sim 300$ Myr.

Figure 10 compares the accretion rate of satellite galaxies to the accretion rate of central galaxies in the control sample at four different epochs. Panel (a) shows the accretion rate at z_{sat} when the galaxy becomes a satellite, while panels (b), (c) and (d) show the accretion rates 200 Myr after z_{sat} , 500 Myr after z_{sat} and 1 Gyr after z_{sat} , respectively. The median z_{sat} values in the four halo mass bins are 0.19, 0.55, 0.59 and 0.99 in increasing order of halo mass.

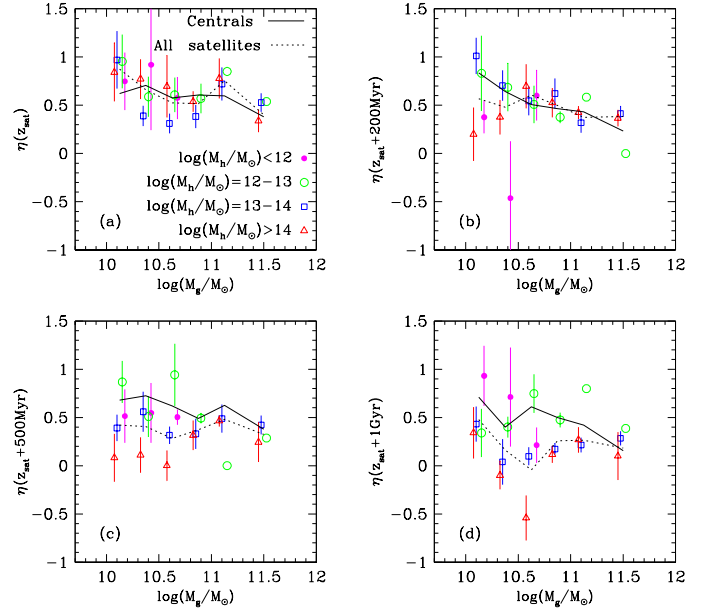


Figure 10. Accretion rate against galaxy mass in bins of 0.25 dex. The top left panel shows the accretion rate at z_{sat} , the epoch at which the galaxy becomes a satellite. The other panels show the accretion rate 200 Myr, 500 Myr and 1 Gyr after z_{sat} . Accretion rate is defined as, $\eta = (\Delta M_{\text{acc}}/M_g) (H^{-1}/t)$ where M_{acc} is the mass accreted in time t , H^{-1} is evaluated at the centre of the time interval, and M_g is the mass of the galaxy at $z = 0$. Lines show the average value for all satellites (dotted) and matched central galaxies (solid) in each galaxy mass bin. Points with error bars show the average value and uncertainty in the mean in four bins of halo mass, as indicated in the legend.

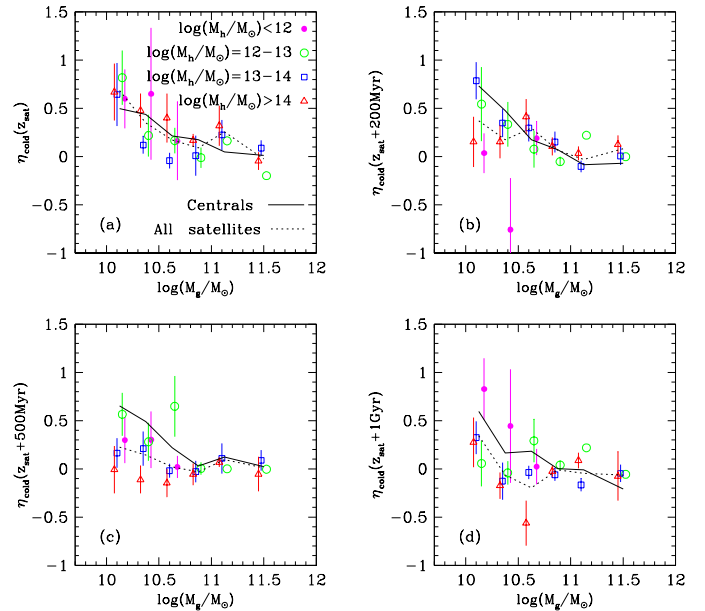


Figure 11. Cold accretion rate vs galaxy mass. This figure is analogous to Figure 10, but showing only cold accretion.

The dotted and solid curves, averaged over all satellites and matched centrals in each galaxy mass bin, afford the best statistics for comparison. At z_{sat} and $z_{\text{sat}} + 200$ Myr, the dimensionless accretion rates of satellite and central galaxies are similar. After 500 Myr, the accretion rates of satellites are systematically lower, and the difference increases at 1 Gyr. Only the lowest mass satellites have significantly non-zero accretion rates at $z_{\text{sat}} + 1$ Gyr. Points with statistical error bars show the accretion rates in bins of halo mass. The drop in satellite accretion rates develops most clearly in the highest mass halo, followed by the next highest mass bin. By $z_{\text{sat}} + 1$ Gyr, some galaxies in the highest mass halo are losing mass. While this analysis would certainly benefit from better statistics (i.e. a larger simulation volume), the trends with time and halo mass are continuous. They indicate that satellite accretion shuts off gradually, over a timescale of 0.5–1 Gyr, with low mass galaxies in high mass haloes showing the strongest effect.

Figure 11 repeats this analysis for cold accretion only. Here the accretion rates are close to zero for all galaxies with M_g above $\sim 10^{10.7} M_\odot$, both central and satellite, at all the epochs shown. At lower M_g , the accretion rates are still significantly reduced relative to Figure 10, but the differences between central and satellite galaxies and the dependence on halo mass are similar. It is particularly notable that low mass satellites in the 10^{13} – $10^{14} M_\odot$ halo mass bin have positive cold accretion rates at $z_{\text{sat}} + 200$ Myr and $z_{\text{sat}} + 500$ Myr. Note, however, that the most massive haloes in the bin are $\sim 3 \times 10^{13} M_\odot$. Even satellites in the $3 \times 10^{14} M_\odot$ halo show cold accretion at z_{sat} and, to a lesser extent, at $z_{\text{sat}} + 200$ Myr.

Besides smooth accretion of gas, galaxies also grow by receiving mergers from lower mass galaxies. Since we do not resolve galaxies below $6 \times 10^9 M_\odot$, we restrict our merger analysis to systems in which the primary galaxy is more massive than $3 \times 10^{10} M_\odot$ and the merger mass ratio is $R_{\text{merg}} \geq 0.25$. As we go to higher redshifts, the galaxy masses decrease, causing the number of resolved mergers to decrease. Hence, we restrict our merger analysis to mergers between $z = 1$ and $z = 0$. The top panel of Figure 12 shows R_{merg} for all merger events between $z = 1$ and $z = 0$ as a function of the $z = 0$ baryonic mass of the galaxy, differentiating between the central/satellite status of the primary galaxy at z_{merg} (the epoch of the merger) and at $z = 0$. We see mergers with a wide range of mass ratios for satellites as well as centrals. A small fraction of mergers ($\sim 10\%$) are between objects of similar mass ($R_{\text{merg}} \geq 0.9$). More than four-fifths of merger events involve a satellite galaxy merging with the central galaxy of its parent halo. About one-third of these galaxies go on to become satellites by $z = 0$, following a merger of their parent halo with a halo hosting a more massive galaxy. However, it is notable that close to one-fifth of the merger events in our simulation are mergers between two satellite galaxies.

The bottom panel of Figure 12 compares the fraction of central and satellite galaxies that receive mergers between $z = 1$ and $z = 0$ above a certain merger ratio, R_{merg} . One-fourth of the galaxies in the simulation (above $3 \times 10^{10} M_\odot$) experience at least one merger with $R_{\text{merg}} \geq 0.25$ between $z = 1$ and $z = 0$. This fraction is similar for central galaxies and for $z = 0$ satellites and the R_{merg} distribution is also similar, as one can see by comparing the solid and dashed

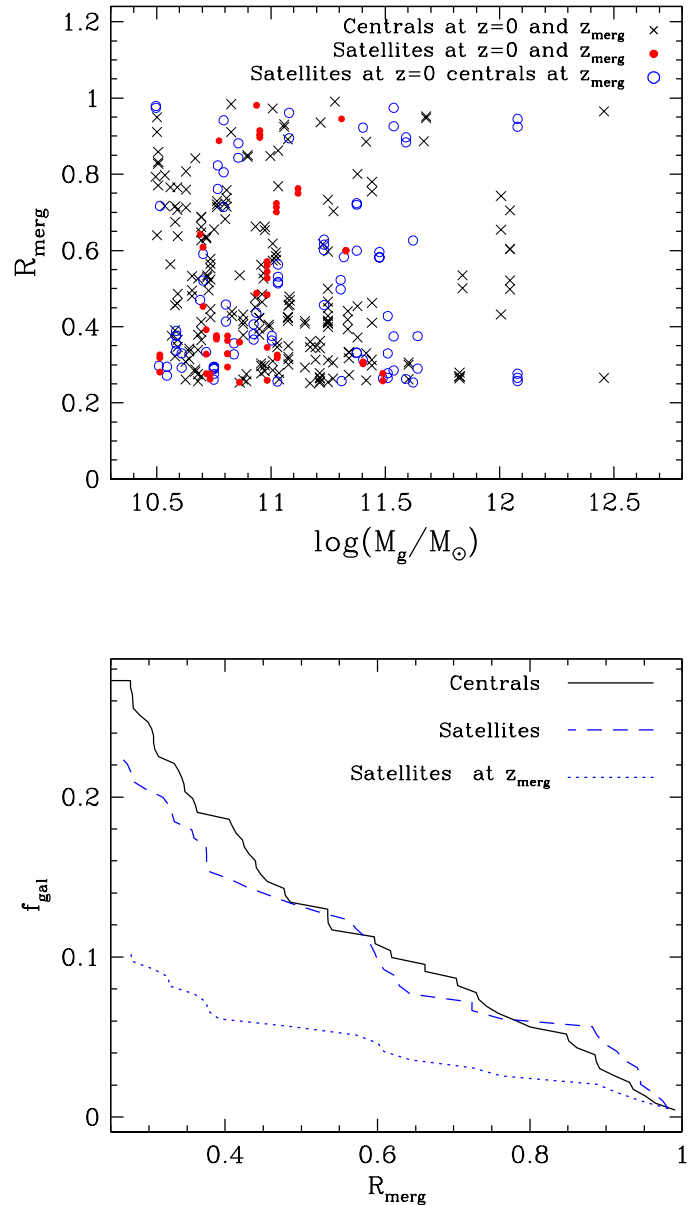


Figure 12. (Top) Merger events after $z = 1$ with mass ratio $R_{\text{merg}} \geq 0.25$, versus galaxy baryonic mass at $z = 0$. Central galaxies, $z = 0$ satellites that are centrals at the merger epoch z_{merg} and galaxies that are satellites at z_{merg} are shown separately, as indicated in the legend. (Bottom) Fraction of central galaxies (solid line), $z = 0$ satellites (dashed line) and galaxies that are satellites at z_{merg} (dotted line) that receive a merger above a certain R_{merg} .

lines. However, the fraction of satellites that receive mergers after z_{sat} is a factor of 2–3 lower (dotted line). Galaxies that receive mergers often receive more than one merger, so the accounting in the top and bottom panels is somewhat different.

Figure 12 adopts the somewhat arbitrary redshift interval $z = 1$ to $z = 0$, and the mass distributions of the central and satellite galaxies are systematically different. To fairly compare the merger activity of central galaxies and post- z_{sat} satellites, we return to the control sample used for our accretion comparisons. The top panel of Figure 13 shows the

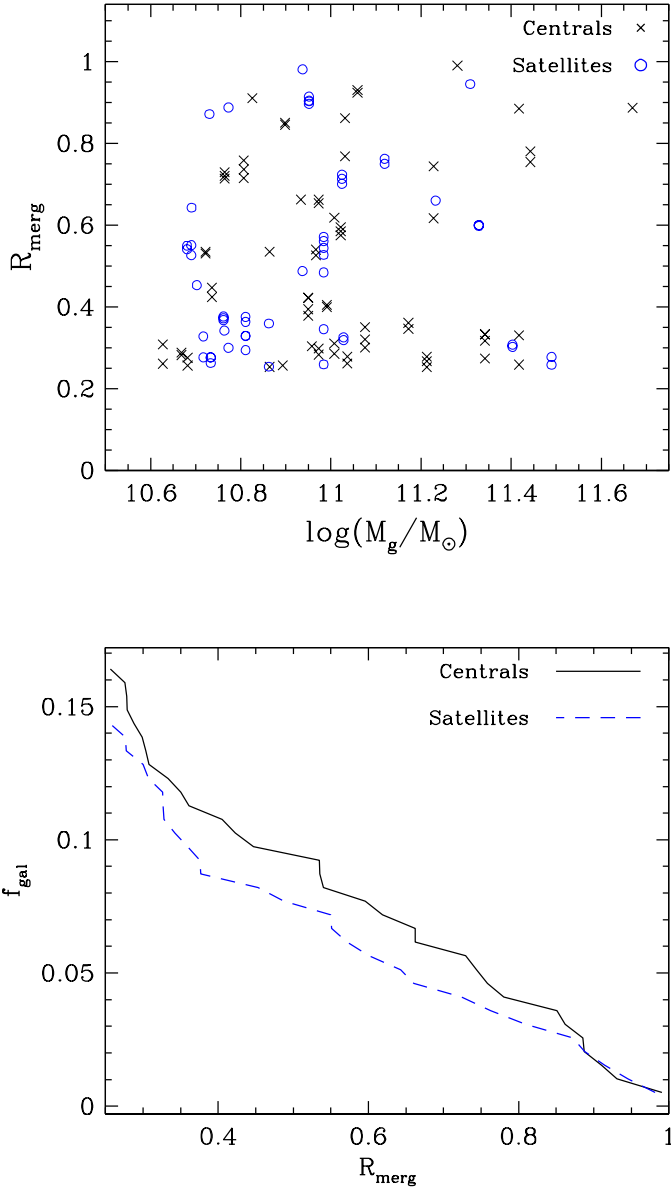


Figure 13. (Top) Merger mass ratio R_{merg} vs $z = 0$ galaxy baryonic mass for mergers received by satellite galaxies after z_{sat} compared to the control sample of central galaxies over the same time period. (Bottom) Fraction of satellite galaxies (dashed line) and central galaxies in the control sample (solid line) that receive a merger above a certain R_{merg} .

merger ratio for mergers (no longer restricted to $z \leq 1$) with $R_{\text{merg}} \geq 0.25$ received by satellite galaxies and by the control sample of central galaxies after z_{sat} of the matched satellite. Only 14% of satellite galaxies and 16% of central galaxies in the control sample receive mergers after z_{sat} . The distribution of mass ratios is broad for both populations. Our sample is not large enough to study the merger properties of satellite galaxies as a function of halo mass. The bottom panel of Figure 13 shows the fraction of central and satellite galaxies that receive a merger above a given R_{merg} after z_{sat} (in contrast to Figure 12, which shows all mergers since $z = 1$ and includes all central galaxies). The probability of a satellite galaxy receiving a merger above a certain mass ra-

tio is only $\sim 2\%$ lower than that of a central galaxy of similar mass, across a wide range of merger mass ratios.

4 DISCUSSION

The central galaxies of haloes form a distinct population in this simulation, as anticipated by semi-analytic models (White & Frenk 1991; Kauffmann, White & Guideroni 1993; Cole et al. 1994) and as found in previous numerical studies (Berlind et al. 2003; Zheng et al. 2005). In the great majority of FOF haloes, the most massive galaxy lies at the bottom of the dark matter potential well and close to the centre of mass. In more than two-thirds of the FOF haloes, the baryonic mass (stars + cold gas) of the central galaxy is 2-5 times higher than that of the most massive satellite. Only a small fraction of FOF haloes host two galaxies of similar mass. Because of its limited volume, our simulation has only one cluster mass halo ($M \sim 3 \times 10^{14} M_\odot$). The other haloes massive enough to host resolved satellites range from $\sim 3 \times 10^{11} M_\odot$ to $\sim 3 \times 10^{13} M_\odot$, while haloes down to $\sim 10^{11} M_\odot$ host resolved central galaxies.

The distinction between central and satellite galaxies in our simulation is weaker than expected in a simple picture where only central galaxies accrete mass and “receive” mergers of less massive systems. Galaxies that are satellites at $z = 0$ assembled their mass earlier, on average, than present day central galaxies of the same baryonic mass, and satellites of more massive haloes have systematically higher assembly redshifts. However, to a large extent the baryonic mass of a galaxy is a better predictor of its accretion and merger history than its central or satellite status, with the exception of galaxies in the cluster mass halo. In part, the dominance of baryonic mass over satellite status just reflects the fact that many satellites were central galaxies for most of their history, merging into larger haloes only at low redshift. However, we find that simulated galaxies continue to accrete gas and, in some cases, merge with lower mass objects even after they become satellites. In essence, galaxies that enter the virial radius of a larger halo may remain the “central” galaxies of their own dark matter substructure, and they lose their central status only gradually. Alternative halo definitions (e.g., higher threshold density or spherical overdensity identification) could yield somewhat sharper distinctions between central and satellite galaxies, but we do not expect them to change this basic result.

While galaxies continue to accrete gas after becoming satellites, they accrete less than a “control” sample of central galaxies with similar baryonic masses measured over the same time period. At the time they enter a larger halo, satellites have similar accretion rates to central galaxies of the same mass, and the accretion rate declines towards zero over the next 0.5-1 Gyr. Lower mass satellites in the cluster mass halo begin to lose mass, and by $z = 0$ they are typically 10-20% less massive than they were when they became satellites. When we compare satellite galaxies to central galaxies of the same baryonic mass, we find large systematic differences if, and only if, the mass of the satellite’s host halo is much larger than the typical halo mass for the corresponding central galaxies.

As in Kereš et al. (2005), we find that galaxies below $M_g \sim 3 \times 10^{10} M_\odot$ accrete predominantly through “cold

mode”, while higher mass galaxies grow mainly through “hot mode” accretion of virial temperature gas. This transition is similar for central and satellite galaxies. Consequently, our general conclusions would still hold if we assumed that a galaxy’s true accretion rate was close to its cold (rather than total) accretion rate, for either the physical or numerical reasons discussed in §3, except that the accretion rates of massive galaxies would become very low. Regardless of whether we consider total accretion or cold accretion only, these simulations exhibit natural “downsizing” in which accretion and star formation shift towards lower mass galaxies at later times (Kereš et al. 2005, 2008).

Comparing present day central galaxies and present day satellites, above a mass threshold of $M_{\text{gal}} = 3 \times 10^{10} M_{\odot}$, we find that only a slightly larger fraction of centrals (27% vs. 22%) have received mergers with mass ratio $R_{\text{merg}} \geq 0.25$ since $z = 1$. Roughly half of the satellite mergers occurred after the larger parent had become a satellite, and half occurred while it was still a central object. The mass ratio distributions are similar in all cases. There are more central galaxies than satellites and only about one in five resolved merger events involves two satellites. However, if we compare satellites to a control sample of centrals as we did for accretion, we find similar fractions experiencing resolved, $R_{\text{merg}} \geq 0.25$ mergers during the course of the simulation, with similar R_{merg} distributions. In summary, most galaxies have quiescent assembly histories at $z < 1$, and the merger rates of central and satellite galaxies are not radically different. The most massive galaxies do have more complex merger histories (Maller et al. 2006), and these are usually central galaxies of high mass haloes.

While we have focused on mass growth rather than star formation, the two are closely linked in our simulation, with star formation generally following gas accretion after a short delay. The fact that galaxies experience continuing gas accretion for 0.5-1 Gyr after becoming satellites means that satellites will be systematically bluer than predicted in semi-analytic models that assume no accretion onto satellites (“strangulation”). There are numerous indications that including the continuing satellite accretion predicted here would improve the match between semi-analytic models and observations. Weinmann et al. (2006) find that the Croton et al. (2006) semi-analytic model predicts an excessive fraction of red satellites relative to the satellite population in groups identified from the Sloan Digital Sky Survey (SDSS). The discrepancy is largest for lower mass groups, which have much higher blue fractions than predicted, consistent with our finding that the central-satellite distinction becomes sharper for satellites in high mass haloes. Li et al. (2007) show that the pairwise velocity distributions predicted by the Kang et al. (2005) and Croton et al. (2006) models can be brought into agreement with SDSS measurements by reducing the fraction of faint red galaxies. Coil et al. (2008) find similar trends at $z \sim 1$, showing that the Croton et al. (2006) model predicts excessive clustering of red galaxies and insufficient clustering of blue galaxies relative to the DEEP2 Galaxy Redshift Survey, especially on small scales. Most recently, Weinmann et al. (2008) show that the colours of SDSS satellites can be reproduced if their star formation slows over a timescale of 2-3 Gyr after z_{sat} , somewhat larger than the timescale for accretion shut off found here.

Other observations indicate that the colours of satellite galaxies depend systematically on halo mass, as we would expect based on the assembly redshift trends in Figures 6 and 8. In a sample of clusters taken from the Red-Sequence Cluster Survey, Gilbank et al. (2008) find that the red fraction in clusters increases with richness, indicating an earlier truncation of star formation in higher mass haloes. Hansen et al. (2007) find a similar result using data from the SDSS. Finally, X-ray studies of clusters indicate that massive satellites retain local concentrations of hot gas (Sun et al. 2007; Jeltama, Binder & Mulchaey 2008), providing further evidence that the physical transition from “central galaxy” to “satellite” is a gradual one. Further discussions of the impact of the halo environment on satellite galaxy properties, focused on the effects of ram pressure stripping, are given by McCarthy et al. (2008) and Font et al. (2008).

Our small simulation volume limits our statistical power, especially for massive haloes. In addition, there are indications that the TreeSPH code used here predicts too much hot gas accretion, and that the entropy conserving SPH formulation of Springel & Hernquist (2002) yields more accurate results (Springel & Hernquist 2002; Kereš et al. 2008; Kereš 2007). Kereš et al. (2008) have recently analysed a simulation of a $50h^{-1}\text{Mpc}$ cube evolved with the entropy conserving SPH code GADGET-2 (Springel et al. 2001), with a similar mass resolution to the simulation analysed here. While they focus mainly on the relative importance of cold and hot accretion in galaxy growth, they also investigate central and satellite accretion, and confirm our main result: satellites experience significant amounts of continuing accretion, and the distinction between central and satellite growth rates is smaller at high galaxy masses and (a point not investigated here) at high redshift. Both our simulation and the Kereš et al. (2008) simulation overpredict the observed galaxy baryonic mass function, probably because they do not include galactic winds that eject accreted material from low and intermediate mass galaxies. Winds will change the relation between accretion rates and star formation rates, and they will affect the accretion rates themselves by altering the local gas supply. However, we do not expect them to alter our qualitative conclusions: the distinction between central and satellite galaxies is fundamental to understanding the galaxy population and its evolution, but differences in their growth rates and hence their physical properties are smooth, not sharp.

ACKNOWLEDGMENTS

We thank Mark Fardal and Ari Maller for useful discussions and technical assistance. This work was supported by NASA Grants NAG5-13308 and NNG04GK68G and by an Ohio State University Graduate Fellowship.

REFERENCES

- Bell, E. F., McIntosh, D. H., Katz, N., & Weinberg, M. D. 2003, *ApJS*, 149, 289
- Berlind, A. A., et al. 2003, *ApJ*, 593, 1
- Binney, J. 1977, *ApJ*, 215, 483

- Binney, J. 2004, MNRAS, 347, 1093 .
- Birnboim, Y. & Dekel, A. 2003, MNRAS, 345, 349.
- Blanton, E. L., Gregg, M. D., Helfand, D. J., Becker, R. H., & Leighly, K. M. 2001, AJ, 121, 2915
- Bower, R. G., Benson, A. J., Malbon, R., Helly, J. C., Frenk, C. S., Baugh, C. M., Cole, S., & Lacey, C. G. 2006, MNRAS, 370, 645
- Cattaneo, A., et al. 2007, MNRAS, 377, 63
- Cen, R., & Ostriker, J. P. 2000, ApJ, 538, 83.
- Coil, A. L., et al. 2008, ApJ, 672, 153
- Cole, S., Aragon-Salamanca, A., Frenk, C. S., Navarro, J. F., & Zepf, S. E. 1994, MNRAS, 271, 781
- Croton, D. J., et al. 2005, MNRAS, 356, 1155
- Croton, D. J., et al. 2006, MNRAS, 365, 11
- Davé, R., Dubinski, J., & Hernquist, L. 1997, New Astronomy, 2, 277
- Dekel, A. & Birnboim, Y. 2006, MNRAS, 368, 2.
- Davis, M., Efstathiou, G., Frenk, C. S., & White, S. D. M. 1985, ApJ, 292, 371
- Dunkley, J., et al. 2008, ArXiv e-prints, 803, arXiv:0803.0586
- Evrard, A. E., Summers, F. J., & Davis, M. 1994, ApJ, 422, 11
- Faber, S. M., et al. 2007, ApJ, 665, 265
- Fall, S.M. & Efstathiou, G. 1980, MNRAS, 193, 189.
- Fardal, M. A., Katz, N., Gardner, J. P., Hernquist, L., Weinberg, D. H., & Davé, R. 2001, ApJ, 562, 605
- Font, A. S., et al. 2008, MNRAS, 1000
- Gelb, J.M. & Bertschinger, E. 1994, ApJ, 436, 467.
- Gilbank, D. G., Yee, H. K. C., Ellingson, E., Gladders, M. D., Loh, Y.-S., Barrientos, L. F., & Barkhouse, W. A. 2008, ApJ, 673, 742
- Hansen, S. M., Sheldon, E. S., Wechsler, R. H., & Koester, B. P. 2007, ArXiv e-prints, 710, arXiv:0710.3780
- Hernquist, L. & Katz, N. 1989, ApJS, 70, 419.
- Jeltema, T.E., Binder, B., & Mulchaey, J.S. et al. 2008, arXiv:0801.2570
- Kang, X., Jing, Y. P., Mo, H. J., Börner, G. 2005, ApJ, 631, 21
- Katz, N. 1992, PASP, 104, 852.
- Katz, N., Hernquist, L., & Weinberg, D. H. 1992, ApJL, 399, L109.
- Katz, N., Weinberg D. H., & Hernquist, L. 1996, ApJS, 105, 19.
- Katz, N., Kereš, D., Dave, R., & Weinberg, D. H. 2003, Rosenberg J.L., Putman M.E., eds, ASSL Vol.281: The IGM/Galaxy Connection. The Distribution of Baryons at $z=0$. pp185+
- Kauffmann, G., White, S. D. M., & Guiderdoni, B. 1993, MNRAS, 264, 201
- Kay, S. T., Pearce, F. R., Jenkins, A., Frenk, C. S., White, S. D. M., Thomas, P. A., & Couchman, H. M. P. 2000, MNRAS, 316, 374
- Kereš, D., Katz, N., Weinberg, D. H., & Davé, R. 2005, MNRAS, 363, 2
- Kereš, D., 2007, PhD Thesis, University of Massachusetts.
- Kereš, D., Katz, N., Fardal, M., Davé, R., & Weinberg, D.H. 2008.
- Kravtsov, A. V., Berlind, A. A., Wechsler, R. H., Klypin, A. A., Gottlöber, S., Allgood, B., & Primack, J. R. 2004, ApJ, 609, 35
- Li, C., Jing, Y. P., Kauffmann, G., Börner, G., Kang, X., & Wang, L. 2007, MNRAS, 376, 984
- Maller, A. H., Katz, N., Kereš, D., Davé, R., & Weinberg, D. H. 2006, ApJ, 647, 763
- McCarthy, I. G., Frenk, C. S., Font, A. S., Lacey, C. G., Bower, R. G., Mitchell, N. L., Balogh, M. L., & Theuns, T. 2008, MNRAS, 383, 593
- Miller, G.E. & Scalo, J.M. 1979, ApJS, 41, 513.
- Murali, C., Katz, N., Hernquist, L., Weinberg, D. H., & Davé, R. 2002, ApJ, 571, 1
- Neistein, E., van den Bosch, F. C., & Dekel, A. 2006, MNRAS, 372, 933
- Primack, J. R., Somerville, R. S., Faber, S. M., & Wechsler, R. H. 1998, Phys.Rep., 307, 15
- Springel, V., Yoshida, N., & White, S. D. M. 2001, New Astronomy, 6, 79
- Springel, V., & Hernquist, L. 2002, MNRAS, 333, 649
- Strateva, I., et al. 2001, AJ, 122, 1861
- Sun, M., Jones, C., Forman, W., Vikhlinin, A., Donahue, M., & Voit, M. 2007, ApJ, 657, 197
- Tegmark, M., et al. 2006, Phys.Rev D, 74, 123507
- White, S.D.M., & Rees, M.J. 1978, MNRAS 183, 341.
- White, S.D.M., & Frenk, C.S. 1991, ApJ, 379, 52.
- Weinberg, D.H., Colombi, S., Davé, R., & Katz, N. 2008, ApJ, 678, 6.
- Weinmann, S. M., van den Bosch, F. C., Yang, X., Mo, H. J., Croton, D. J., & Moore, B. 2006, MNRAS, 372, 1161
- Weinmann, S. M., Kauffmann, G., van den Bosch, F. C., Pasquali, A., McIntosh, D. H., Mo, H., Yang, X., & Guo, Y. 2008, ArXiv e-prints, 809, arXiv:0809.2283
- Zheng, Z., et al. 2005, ApJ, 633, 791